# ARTIFICIAL INTELLIGENCE FOR WELL INTEGRITY MONITORING BASED ON EM DATA

**Seyed Ehsan Hosseini[1*], Simone Zonetti[2], Anouar Romdhane[3], Bastien Dupuy[3], Børge Arntsen[1]**

[1] NTNU, Trondheim, Norway

[2] SINTEF Digital, Oslo, Norway

[3] SINTEF Industry, Trondheim, Norway

* Corresponding author e-mail: seyed.e.hosseini@ntnu.no

## Abstract

Monitoring of integrity of plugged and abandoned (P&A'ed) wells is of interest for the oil and gas industry and for CO2 storage. The purpose of this study is to develop artificial intelligence (AI)-based approaches to detect anomalies or defects when monitoring permanently plugged wells. The studied solution is based on the analysis of electromagnetic (EM) data. We consider an offshore setting where the EM signal is generated in presence of a P&A'ed well and the resulting electric field is recorded at the seafloor. Numerical simulations are used to train an AI algorithm to classify the modelled EM features into predefined well integrity classes. We consider four scenarios: (1) no well, (2) well with three 20 meters thick cement barriers of thickness, (3) well with three cement barriers of 60 meters thickness, and (4) well with three cement barriers of 100 meters thickness. Convolutional neural networks (CNNs) are tested as the AI algorithm in this study. After training the algorithm on 80% of the data, it shows an accuracy of 95.36% on the test data. P&A'ed well integrity monitoring currently remains limited to local observation and symptom identification, but this study shows that there is great potential for developing remote non-invasive well integrity monitoring techniques.

***Keywords:*** *P&A'ed well integrity, non-invasive monitoring, electro-magnetic fields, Artificial intelligence, Convolutional Neural Networks (CNNs)*

## 1. Introduction

A well needs to be permanently plugged and abandoned (P&A'ed) when its productive life is over. Several cement plugs are installed in discrete sections of the wellbore. They seal the well structure both vertically and horizontally [1]. Moreover, the wellhead is detached, and the top portion of the well is severed several meters below the seafloor (Figure 1). Nowadays, this technique is used to prevent long-term leakage.

Heat, pressure, corrosion, seismic activity, subsidence, and formation creep exert strong mechanical loads on the wellbore construction over time [2]. It is estimated that well which reached 15 years of age might have a 50% probability of leakage [3]. It is reported that 0.9-3.7 kt $yr^{-1}$ of $CH_4$ is emitted from 1,792 wells in an area of 20,000 $km^2$ in the UK sector of the central North Sea, suggesting that the large number of wells in North Sea likely constitute a major source of methane [4]. In Pennsylvania, 6% of the methane emissions have been associated to leakage from old wells [5]. At the Groningen field in the Netherlands, 1 out of 29 wells was found to be leaking [6].

There is a need for monitoring the integrity of P&A'ed wells. As the wellhead and top pipes are removed and buried in sediments, it is difficult and expensive to use logging tools to monitor well integrity. Thus, "post-mortem" monitoring of leakage is the only possible option with observations of bubbles or growth of bacterial mats at the seafloor in the vicinity of the well [7].

Although recent studies emphasize developing non-invasive well integrity monitoring methods [2][8], all of the current methods are variations of permanent sensing systems which monitor some parameters such as temperature, strain, pressure, chemical and acoustic sensing. They can be used both in a point sensing manner or in a distributive manner along the entire well.

There are some options for non-invasive well integrity monitoring that can be developed. One of them is acoustic systems which use guided waves for high-resolution imaging. Although these systems are already used for monitoring the pipelines in aircraft industry [9][10], they have not been customized for well integrity monitoring. They can be used at the surface of the casing or in the well's internal casing. As P&A'ed wells are cut below the seafloor, these methods are more difficult to implement because they require access to well casings.

Another option for both temporarily and permanently plugged wells is based on electric and magnetic fields. They have already seen great success in geophysical imaging of the subsurface. Magnetotellurics (MT), magnetometric resistivity (MMR), electrical resistivity tomography (ERT), and controlled-source electromagnetics (CSEM) are based on using passive or active electric-magnetic fields in different frequency bands. These systems have already some commercial applications such as hydrocarbon exploration [11], large

scale crustal imaging [12], and CO2 storage monitoring [13][14]. Nowadays, researchers show their interest to use these systems for well integrity measurements. One example is using CSEM surveys for casing integrity measurements where steel casing is used as electrodes during CSEM surveys [15][16].

In this paper, we propose an AI algorithm which senses changes in a well structure based on seabed electric field. In the proposed method detailed in section 2, the electric field at the seabed is simulated using a finite-element simulator. We consider four scenarios, with no well in one of them, and thickness of cement plugs inside the wellbore changed for the three others. Then, a carefully designed CNN algorithm is trained to discriminate them. The methodology is described in section 2 and the results presented and discussed in section 3.

## 2. Method

### *2.1 Geometry*

Here we consider a simplified well geometry consisting of a 700-meter cylinder with radius of 20 cm (Figure 2). The inner hole is filled with 9 cm brine/sea water, 1 cm metal casing, and 10 cm of cement. In addition, horizontal elements that simulate the presence of cement plugs can be introduced in the well. The well elements are placed within a large, cylindrical modelling domain with radius of several hundreds of meters. The modelling domain is layered horizontally to include a 100 m air layer at the top, a 100 m sea water layer below, and a 900 m layer of rock formation, which can fully enclose the well element. The well-head can be placed at any location at or below the sea floor. An additional geometric layer surrounds the modelling domain to apply Infinite Element Domains (absorbing boundary conditions) features in the simulation software.

### *2.2 Materials*

In the implementation of the model, all material properties are frequency independent. This is an approximation that will be relaxed in subsequent work in order to optimize the detected signal depending on the frequency of the source. Furthermore, the materials are assumed to be perfectly homogeneous and isotropic. This can be easily relaxed by introducing both diffuse inhomogeneity and material property gradients, especially in the rock formation. Table 1 gives a summary of the EM material properties for the well elements.

### *2.3 Electromagnetic signals*

Electromagnetic signals are excited in the model via a 1 m long perfectly conducting dipole, which can be placed anywhere in the geometry. By simulating tangential and radial polarizations for the transmitter, we can take advantage of field symmetry to reduce the modelling domain to ½ of the original, reducing computational requirements. The vertical position of the dipole is a free parameter, and it has been fixed to 30 m below the water surface. The position of the source and receivers can be adapted depending on EM measurements providers. With no dependence of material properties on frequency nor field strength, the problem is linear with respect to the field amplitude, and therefore the transmitter is driven with a constant current of nominal amplitude. The operating frequency is correspond to 0.5 Hz. A schematic representation of the geometry used is provided in Figure 2. The electrical properties of the different components are also given in Table 1.

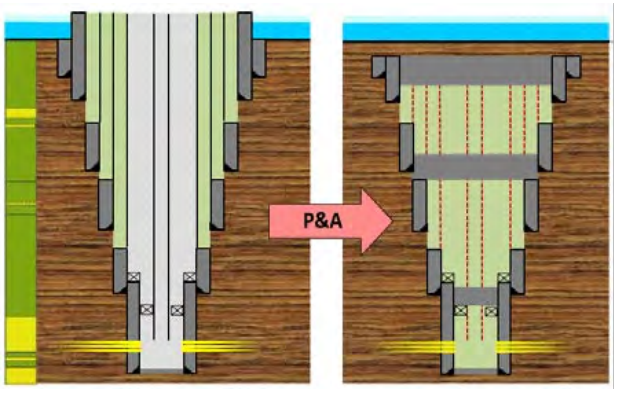


Figure 1: A typical well before (left) and after (right) permanent well plugging [2]. Cement barriers are grey in the figure.

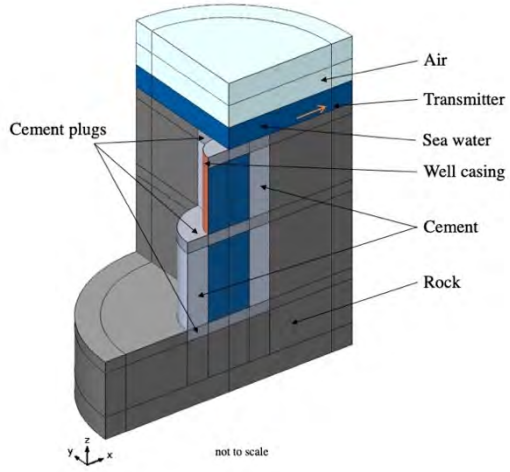


Figure 2: Schematic representation of the model's geometry, including well casing, three cement plugs and a well head at the sea floor.

Table 1: Material properties.

| Material | Electrical properties | |
|---|---|---|
| | Conductivity [S/m] | Relative permittivity [F/m] |
| Rock formation | 0.50 | 6 |
| Cement | 0.33 | 2.20 |
| Steel | 62500 | 1 |
| Sea Water | 3 | 78.40 |
| Air | 0 | 1 |

### *2.4 FEM implementation*

The model is implemented using the commercial Finite Element Method (FEM) software COMSOL Multiphysics [17]. Given the operating frequency of 0.5 Hz, resulting in a local wavelength much larger than the size of the modelling domain, inductive effects can be neglected in the first approximation, and one can take advantage of the simplified formulation of Maxwell's equations implemented in the Electric Currents interface. The Infinite Element Domains feature can be the external domains of the geometry, allowing simulated fields to vanish at infinity and avoid fields reflections at the sides of the simulation model. The electrically thin steel casing at the interface between sea water (inside the well) and cement is simulated using the dedicated Distributed Impedance boundary condition, which effectively simulates the 1 cm thick material as a 2D surface, thus eliminating the need of meshing the thickness of this layer. The interior of the model is meshed using triangular elements on the sea floor surface (Figure 3), on which a tetrahedral mesh is built in the sea water domain. Mesh elements are kept small enough close to the well to ensure a sufficient discretization of the immediate vicinities of the well itself. The annulus element around the sea floor uses a mapped mesh, while the rest of the mesh is swept vertically from the top and bottom boundaries of the water layer.

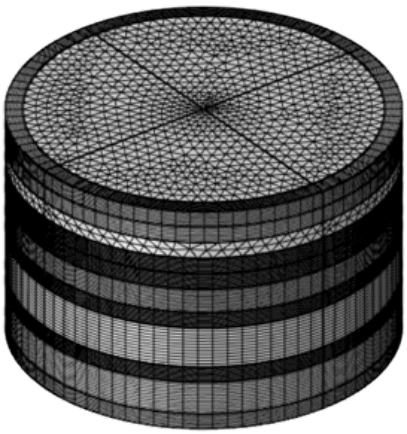

Figure 3: Example of meshed modelling domain for FEM simulations.

### *2.5 AI algorithm*

CNN [18] is the AI algorithm which is used in this study for classification among four different scenarios including: (1) Case A: No well, (2) Case B: A well with three 20-meter cement plugs inside the wellbore, (3) Case C: a well with three 60-meter cement plugs inside the wellbore, and (4) Case D: a well with three 100-meter cement plugs inside the wellbore. The aim of the AI algorithm is to discriminate among these four scenarios using as input the electric field simulated at the seabed. The CNN structure used in this research consists of 3 blocks of convolution and 2 fully connected layers with 64 and 4 neurons respectively (Figure 4). Each of the convolutional blocks has Relu activation function [19], and a Max-Pooling of 2 by 2 [20]. The last layer has SoftMax activation function to report the uncertainty associated with the obtained classification. For more generalization of the network, Dropout is employed [21]. Dropout rate is 0.2 in each convolutional block (between convolution and Max-pooling layer), and it is 0.5 before the last layer.

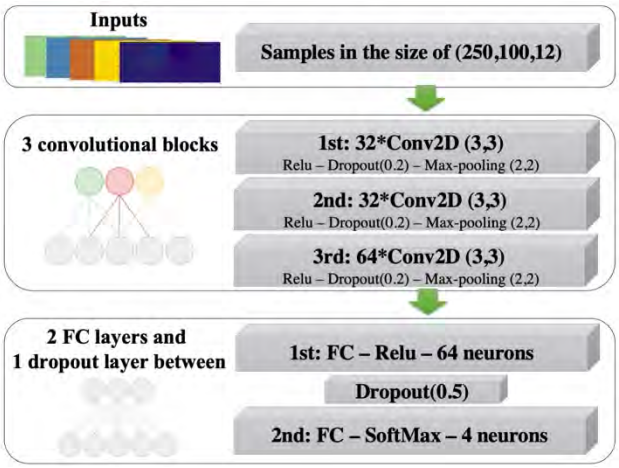


Figure 4: Proposed convolutional neural network structure.

### *2.6 Preprocessing and data augmentation*

Since neural networks need some data to learn, different orientations of transmitter dipole antenna are used to augment the data. For each scenario, the antenna direction is changed from x-direction to y-direction with a step of one degree. Thus, there are 91 electric field data for each scenario (364 samples overall). 12 features are taken out from these electric fields including: real part, imaginary part, magnitude, and phase of electric fields in each direction. Since it would be hard to measure electric field at the seabed, we constrain the span of received electric field. We do this by cropping an area with the size of 250 by 100 meters around the well. Then, all features get sparse by setting 7/8 of values in x direction and 4/5 of values in y direction to zero (meaning no measurements at those locations). Finally, values are scaled between -1 and +1 to allow for better training in our neural network (Figure 5). These data are labeled and used to train and test our classification method. One feature map of an input sample is provided in Figure 6 for illustration.

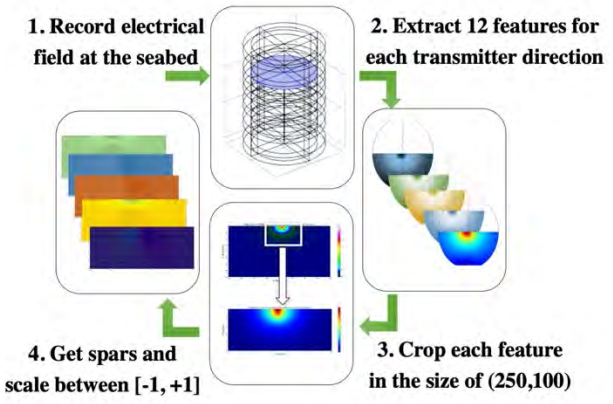


Figure 5: Preprocessing workflow.

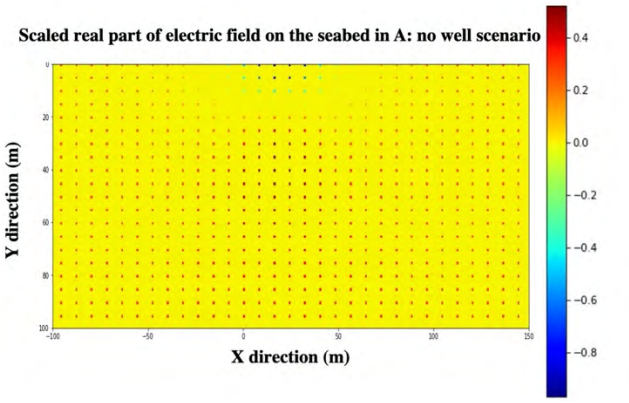


Figure 6: Example of an input feature to the CNN.

## 3. RESULTS

After simulating electric fields with FEM, CNN is trained in 50 epochs with batch-size of 16. To ensure that no overlap occurs between training and test content, the augmented data was divided into 80% (291 samples) for training and 20% (73 samples) for testing. Since artificial neural networks use randomness (random initial weights, shuffling, etc.) during each training epoch, a repeated stratified five-folded cross-validation is introduced to build more robust results. It means that training and testing were implemented 5 times with different test data each time. Moreover, the whole process is repeated and implemented 30 times, resulting in a more reliable evaluation of the model performance. The overall confusion matrix for all the test data after repeated stratified five-folded cross-validation is shown in Table 2. This table tells how our classification method predicts each class label after training is performed.

Table 2: Derived confusion matrix. A: no well, B: a well with three 20-meter cement plugs inside the wellbore, C: a well with three 60-meter cement plugs inside the wellbore, and D: a well with three 100-meter cement plugs inside the wellbore.

| | | Predicted Label | | | |
|---|---|---|---|---|---|
| | | A | B | C | D |
| True Label | A | 2526 | 71 | 1 | 132 |
| | B | 19 | 2685 | 1 | 25 |
| | C | 13 | 5 | 2651 | 61 |
| | D | 96 | 56 | 27 | 2551 |

The classifier is tested on 10920 test samples which consists of 364 unique test samples. These unique test samples are evaluated on 30 different CNNs. Table 2 shows a very low misclassification rate as most samples are classified correctly. Although the AI algorithm shows more misclassification in class (D), it shows a robust performance, and it can classify each scenario very well. In order to understand how well each scenario is classified, a normalized confusion matrix (based on each row) is drawn in Table 3 with the corresponding percentages.

Table 3: Normalized confusion matrix. Numbers are provided in percentage in the table. A: no well, B: a well with three 20-meter cement plugs inside the wellbore, C: a well with three 60-meter cement plugs inside the wellbore, and D: a well with three 100-meter cement plugs inside the wellbore.

| | | Predicted Label | | | |
|---|---|---|---|---|---|
| | | A | B | C | D |
| True Label | A | 92.53 | 2.60 | 0.03 | 4.84 |
| | B | 0.70 | 98.35 | 0.03 | 0.92 |
| | C | 0.48 | 0.18 | 97.11 | 2.23 |
| | D | 3.52 | 2.05 | 0.99 | 93.44 |

Table 3 shows how well our method classifies each scenario. For instance, 92.53% of real data in scenario (A) is predicted as scenario (A). Similarly, 2.60% of real data in scenario (A) is classified as scenario (B). By looking at this table, it is obvious that scenario (A) and (D) are more prone to misclassification as the misclassification error is higher. Evaluation metrics of our classifier are provided in Table 4 (numbers in percentage). Table 4 shows classification metrics not only in each class but also in average which is based on macro- and micro-average method. Since micro-average method is more reliable than macro-average, we report our final results based on it. The overall accuracy of our classification method is 95.36% with standard deviation of 1.45% after training 30 times on different initialized models.

Table 4: Evaluation metrics of our classifier (percentages). A: no well, B: a well with three 20-meter cement plugs inside the wellbore, C: a well with three 60-meter cement plugs inside the wellbore, and D: a well with three 100-meter cement plugs inside the wellbore.

| | Precision | Recall | F1-score | Accuracy |
|---|---|---|---|---|
| A | 95.18 | 92.53 | 93.83 | 96.96 |
| B | 95.31 | 98.35 | 96.81 | 98.38 |
| C | 98.92 | 97.11 | 98.00 | 99.01 |
| D | 92.13 | 93.44 | 92.78 | 96.36 |
| Macro-Ave | 95.38 | 95.36 | 95.37 | 97.68 |
| Micro-Ave | 95.36 | 95.36 | 95.36 | 95.36 |

## 4. Conclusions

Remotely inspecting a subsea well and its structure remains limited to symptom identification around the well. By using a simple geometry and the power of deep neural networks, this study shows that it would be possible to classify plugging thickness under the seabed from recorded EM fields. The accuracy of 95.36% in our neural network-based classifier proves this claim. Our proposed method can distinguish among four different

scenarios related to changes in a wellbore by using just finite sparse electric fields at the seabed.

We aim at developing a generalized AI anomaly detection algorithm that uses different types of data (seismic, EM, etc.) recorded remotely to detect the changes in the cement plugs of a well and not just classifying some scenarios. Moreover, we will not limit the method to one specific well and we will consider more realistic models. The effects of data noise and uncertainty related to the rock formation properties will be analyzed in the future work. Evaluating other types of data, like acoustic data for well monitoring and analyzing the method in detection of some leaking scenarios will also be considered.

Although the assumptions used like considering a simple geometry or using known medium properties in this study, we believe that it will pave the way for further investigating the potential of non-invasive well integrity monitoring techniques that would be applicable also for P&A'ed wells. Accordingly, it would take the industry from a reactive state (symptom detection) to proactive state (take action before leakage occurs).

## Acknowledgements

This work is performed with support from the Research Council of Norway (TOPHOLE project Petromaks2-KPN 295132) and the NCCS Centre (NFR project number 257579/E20).

## References

[1] Vrålstad, T., Saasen, A., Fjær, E., Øia, T., Ytrehus, J. D., & Khalifeh, M. (2019). Plug & abandonment of offshore wells: Ensuring long-term well integrity and cost-efficiency. Journal of Petroleum Science and Engineering, 173, 478-491.

[2] A. Lavrov, M. Torsæter, Physics and Mechanics of Primary Well Cementing, Springer 2016.

[3] C. Brufatto, J. Cochran Aberdeen, S. Lee Conn David Power, S. Zaki Abd Alla El-Zeghaty, B. Fraboulet, T. Griffin, S. James Trevor Munk, F. Justus Santa Cruz, B.R. Joseph Levine, C. Montgomery, D. Murphy, J. Pfeiffer Houston, T. Tiraputra Pornpoch, L. Rishmani Abu Dhabi, From Mud to Cement Building Gas Wells, Oilf. Rev. (2003) 62–76.

[4] Böttner, C. et al., "Greenhouse gas emissions from marine decommissioned hydrocarbon wells: leakage detection, monitoring and mitigation strategies", International Journal of Greenhouse Gas Control, 100 (September 2019), p. 103119.

[5] T. H. Darrah, A. Vengosh, R. B. Jackson, N. R. Warner, R. J. Poreda. Noble gases identify the mechanisms of fugitive gas contamintaion in drinking-water wells overlying the Marcellus and Barnett Shales. PNAS 111,39 (2014) 14076-14081.

[6] G. Cardon de Lichtbuer. Methane leakage from abandoned gas wells in the Netherlands, reality or fiction Master Thesis University of Utrecht, 2017-2018. Available at: https://dspace.library.uu.nl/bitstream/handle/1874/356894/Thesis%20Guillaume.pdf?sequence=2&isAllowed=y

[7] L. Vielstädte, M. Haeckel, J. Karstens, P. Linke, M. Schmidt, L. Steinle and K. Wallmann. Dealing with legacy wells: Implications from subsea leakage along amabdoned North Sea gas wells. Presented at 11th IEAGHG Monitoring Network Meeting, 13-15th June 2017. Available at: https://ieaghg.org/docs/11mon/Session11_Talk1_IEAGHG_lvielstaedte.pdf

[8] Pinto, H.L. and P.M. Gouvea. Well Integrity Monitoring: Challenges and Perspectives. in OTC Brasil. 2013: Offshore Technology Conference.

[9] Rose, J.L., A baseline and vision of ultrasonic guided wave inspection potential. Journal of pressure vessel technology, 2002. 124(3): p. 273-282.

[10] Rocha, B., C. Silva, and A. Suleman, Structural health monitoring system using piezoelectric networks with tuned lamb waves. Shock and Vibration, 2010. 17(4-5): p. 677-695.

[11] Constable, S. (2010) 'Ten years of marine CSEM for hydrocarbon exploration', *Geophysics*, 75(5).

[12] Bai, D. et al. (2010) 'Crustal deformation of the eastern Tibetan plateau revealed by magnetotelluric imaging', Nature Geoscience, 3(5), pp. 358–362.

[13] Michelle Ellis and Martin Sinha, (2010), "The potential of controlled source electromagnetic surveying in CO 2 storage monitoring," SEG Technical Program Expanded Abstracts: 843-847.

[14] Kang, S. et al. (2015) 'MCSEM inversion for CO2 sequestration monitoring at a deep brine aquifer in a shallow sea', Exploration Geophysics, 46(3), pp. 236–252.

[15] Tietze, K., Ritter, O., Veeken, P., & Verboom, B. (2015). CSEM for monitoring reservoir oil-saturation using a borehole-to- surface set-up. In SEG Technical Program Expanded Abstracts 2015 (pp. 937-941). Society of Exploration Geophysicists.

[16] Daley, T. M., Marchesini, P., Wilt, M., Cook, P., Freifeld, B. M., & Lawton, D. (2017). Containment and Monitoring Institute- Baseline Geophysics for CO2 Monitoring with Crosswell Seismic and Electromagnetics. In EAGE/SEG Research Workshop 2017.

[17] COMSOL Multiphysics® v. 5.4. www.comsol.com. COMSOL AB, Stockholm, Sweden.

[18] Yamashita, R., Nishio, M., Do, R.K.G. *et al.* Convolutional neural networks: an overview and application in radiology. *Insights Imaging* 9, 611–629 (2018).

[19] G. E. Dahl, T. N. Sainath, and G. E. Hinton, "Improving deep neural networks for lvcsr using rectified linear units and dropout," in ICASSP, 2013, pp. 8609–8613.

[20] J. Nagi *et al.*, "Max-pooling convolutional neural networks for vision-based hand gesture recognition," *2011 IEEE International Conference on Signal and Image Processing Applications (ICSIPA)*, Kuala Lumpur, 2011, pp. 342-347, doi: 10.1109/ICSIPA.2011.6144164.

[21] Nitish Srivastava et al., "Dropout: A Simple Way to Prevent Neural Networks from Overfitting," Journal of Machine Learning Research 15 (2014): 1929–1958.